Far-field radiation from seismic sources in 2D attenuative anisotropic media

Yaping Zhu and Ilya Tsvankin
Center for Wave Phenomena, Department of Geophysics, Colorado School of Mines, Golden, CO 80401-1887

ABSTRACT
Anisotropic attenuation may strongly influence the energy distribution along the wavefront, which has serious implications for AVO (amplitude-variation-with-offset) analysis and amplitude-preserving migration. Here, we present an asymptotic (far-field) study of 2D radiation patterns for media with anisotropic velocity and attenuation functions.
An important parameter for wave propagation in attenuative media is the angle between the wave and attenuation vectors, which is called the "inhomogeneity angle." Application of saddle-point integration helps us to evaluate the inhomogeneity angle and test the common assumption of "homogeneous" wave propagation that ignores the misalignment of the wave and attenuation vectors. For transversely isotropic media, the inhomogeneity angle vanishes in the symmetry directions and remains small if the model has weak attenuation and weak velocity and attenuation anisotropy. However, reflection and transmission at medium interfaces can substantially increase the inhomogeneity angle, which has an impact on both the attenuation coefficients and radiation patterns. Numerical analysis indicates that the attenuation vector deviates from the wave vector in the direction of increasing attenuation.
The combined influence of angle-dependent velocity and attenuation results in pronounced distortions of radiation patterns, with the contribution of attenuation anisotropy rapidly increasing as the wave propagates away the source. Our asymptotic solution also helps to establish the relationships between the phase and group parameters when wave propagation cannot be treated as homogeneous. Whereas the phase and group velocities are almost independent of attenuation, the inhomogeneity angle has to be taken into account in the relationship between the phase and group attenuation coefficients.

Key words: attenuation, attenuation anisotropy, point-source radiation, inhomogeneity angle, group attenuation, transverse isotropy

1 INTRODUCTION

Directional variation of attenuation, along with that of velocity, influence the amplitudes and polarizations of seismic waves. In particular, attenuation anisotropy may strongly distort radiation patterns and, therefore, the results of amplitude-variation-with-offset (AVO) analysis.

To analyze wave propagation in attenuative media, both the stiffness coefficients and the wave vector have to be treated as complex quantities. In the presence of attenuation, the directions of the real and imaginary parts of the wave vector $\mathbf{k}$ generally differ from each other, which means that the planes of constant phase and constant amplitude do not coincide (Borcherdt and Wennerberg, 1985; Borcherdt et al., 1986; Krebes and Slawinski, 1991; Krebes and Le, 1994). The angle between the real and imaginary parts of $\mathbf{k}$ is called the "inhomogeneity angle". For plane waves in attenuative media, a wide range of values of inhomogeneity angle

satisfy the Christoffel equation, except for certain "forbidden" directions (Krebes and Le, 1994; Carcione and Cavallini, 1995; Červený and Pšenčík, 2005). To avoid complications associated with the inhomogeneity angle, wave propagation is often treated as "homogeneous", which implies that the real and imaginary parts of the wave vector are parallel to each other (e.g., Zhu and Tsvankin, 2006).

Because different choices of the inhomogeneity angle yield different plane-wave properties, the inhomogeneity angle is an important free parameter for plane-wave propagation. The energy (hence the attenuation behavior) of a wave excited by a seismic source, however, is determined by the boundary conditions, so the inhomogeneity angle is constrained as well. For reflected and transmitted waves, the inhomogeneity angle can be found from Snell's law, which requires that the projection of the complex wave vector onto the interface is preserved (e.g., Hearn and Krebes, 1990; Carcione, 2001).

Point-source radiation patterns in elastic anisotropic media, based on high-frequency asymptotics, have been extensively discussed in the literature (e.g., Tsvankin and Chesnokov, 1990; Gajewski, 1993). Hearn and Krebes (1990) describe ray tracing for inhomogeneous wave propagation in a medium consisting of a stack of isotropic attenuative layers, with the inhomogeneity angle obtained by the method of steepest descent for the stationary rays (i.e, the rays that satisfy Fermat's principle). Krebes and Slawinski (1991) find that method more accurate than an alternative approach that assigns parameters for the initial ray segment emerging from the source in a non-attenuative region.

In this paper, we extend the steepest descent method to wavefields from seismic sources in 2D homogeneous media with anisotropic velocity and attenuation functions. To evaluate the far-field displacement represented with a contour integral, we apply the saddle-point condition to the phase function expressed through the polar angle. This asymptotic solution and numerical examples allow us to evaluate the magnitude of the inhomogeneity angle and its influence on the radiation patterns and phase and group attenuation coefficients.

2 INHOMOGENEITY ANGLE

The wavefield in 2D attenuative anisotropic media can be represented through an integral in the frequency-wavenumber domain (equation A2). In the high-frequency limit, this integral can be evaluated using the steepest-descent method. In the polar coordinate system, the saddle-point condition for the phase function (equation A7) yields a complex value $\tilde{\theta}_s$ of the polar angle (the $\tilde{}$ sign denotes a complex value). The expression for the saddle point $\tilde{\theta}_s$ (equation A8) is a generalization of the corresponding elastic case; the real-valued polar angle and slowness are replaced by their complex counterparts. Thereafter, we will call the imaginary part of the wave vector $\mathbf{k}$ the *attenuation vector*, and the real part of $\mathbf{k}$ simply the *wave vector*. The wave vector and attenuation vector are then determined from $\tilde{\theta}_s$ and the complex slowness $\tilde{p}_s$. The latter is obtained from the Christoffel equation for attenuative media.

Note that neither the real nor imaginary part of $\tilde{\theta}_s$ is the angle of either the wave vector or the attenuation vector. Similarly, neither the real nor imaginary part of $\tilde{p}_s$ is the magnitude of either the wave vector or the attenuation vector. The angle and magnitude of both the wave vector and the attenuation vector can be obtained from $\tilde{\theta}_s$ and $\tilde{p}_s$ in the following way.

We denote the magnitude of the real-valued slowness vector by $p = \dfrac{k}{\omega}$ and the magnitude of the frequency-normalized attenuation vector by $p^I = \dfrac{k^I}{\omega}$, where ω is the angular frequency, $k = |\mathbf{k}|$ is the magnitude of the wave vector $\mathbf{k}$, and $k^I = |\mathbf{k}^I|$ is the magnitude of the attenuation vector $\mathbf{k}^I$. The components of $\tilde{p}_s$ are then rewritten as

$$\tilde{p}_1 = p\sin\theta + ip^I\sin\theta^I; \quad \tilde{p}_3 = p\cos\theta + ip^I\cos\theta^I, \quad (1)$$

where θ and θ^I are the angles between vertical and the wave and attenuation vectors, respectively. Jointly solving equations 1 and A9 yields

$$p = \pm\sqrt{p_s^2\cosh^2\theta_s^I + (p_s^I)^2\sinh^2\theta_s^I}, \quad (2)$$

$$p^I = \pm\sqrt{(p_s^I)^2\cosh^2\theta_s^I + p_s^2\sinh^2\theta_s^I}, \quad (3)$$

$$\tan\theta = \frac{p_s\sin\theta_s\cosh\theta_s^I - p_s^I\cos\theta_s\sinh\theta_s^I}{p_s\cos\theta_s\cosh\theta_s^I + p_s^I\sin\theta_s\sinh\theta_s^I}, \quad (4)$$

$$\tan\theta^I = \frac{p_s^I\sin\theta_s\cosh\theta_s^I + p_s\cos\theta_s\sinh\theta_s^I}{p_s^I\cos\theta_s\cosh\theta_s^I - p_s\sin\theta_s\sinh\theta_s^I}, \quad (5)$$

where $p_s = \mathrm{Re}[\tilde{p}_s]$, $p_s^I = \mathrm{Im}[\tilde{p}_s]$, $\theta_s = \mathrm{Re}[\tilde{\theta}_s]$, and $\theta_s^I = \mathrm{Im}[\tilde{\theta}_s]$. The inhomogeneity angle is then given by $\theta^I - \theta$. For elastic media, both $\tilde{p}_s$ and $\tilde{\theta}_s$ become real values and equations 4 and 5 yield $\theta^I - \theta = 90^\circ$.

When the medium is not just attenuative, but also anisotropic, the complex slowness varies with respect to the complex polar angle at the saddle point ($\left.\dfrac{d\tilde{p}_s}{d\theta}\right|_{\theta=\tilde{\theta}_s} \neq 0$). If the medium is homogeneous and isotropic for both velocity and attenuation, equation A8 has a real-valued solution

$$\tilde{\theta}_s = \frac{x_1}{x_3}, \quad (6)$$

so that $\theta_s = \dfrac{x_1}{x_3}$ and $\theta_s^I = 0$. We then find from equations 4 and 5 that $\theta = \theta^I = \theta_s$, which implies the inhomogeneity angle in homogeneous media with isotropic velocity and attenuation is always zero.

3 VTI MEDIA WITH VTI ATTENUATION

3.1 SH-waves

For attenuative media with an anisotropic velocity function, the inhomogeneity angle generally does not vanish. The exact saddle-point condition for SH-waves in VTI (transverse isotropy with a vertical symmetry axis) media with VTI attenuation takes the form

$$\tan\tilde{\theta}_s = \frac{x_1}{x_3(1+2\gamma)}\frac{1-\dfrac{i}{Q_{55}}}{1-i\dfrac{1+\gamma_Q}{Q_{55}}}, \tag{7}$$

where γ_Q is the SH-wave attenuation-anisotropy parameter (equation B3). Clearly, $\gamma_Q = 0$ yields a real-valued $\tilde{\theta}_s$ and results in homogeneous wave propagation. Equation 7 (as well as equations 11 and 12 below) shows that the imaginary part of $\tilde{\theta}_s$ is generally a small quantity proportional to the inverse Q factor.

Using equations A9, 1, and 7, we find for the inhomogeneity angle of the SH-wave:

$$\begin{aligned}&\sin\theta\cos\theta + \mathcal{A}_{SH}^2\sin\theta^I\cos\theta^I\\ &= \mathcal{A}_{SH}\sin(\theta^I-\theta)\frac{1-(1+\gamma_Q)/Q_{55}^2}{\gamma_Q/Q_{55}},\end{aligned} \tag{8}$$

where the normalized phase attenuation coefficient $\mathcal{A} \equiv \dfrac{k^I}{k} = \dfrac{p^I}{p}$ itself is a function of inhomogeneity angle (Zhu and Tsvankin, 2006). For weakly attenuative media ($1/Q_{55} \ll 1$) with weak velocity and attenuation anisotropy ($|\gamma| \ll 1$ and $|\gamma_Q| \ll 1$), the inhomogeneity angle can be simplified by dropping all quadratic terms in Q_{55}, γ, and γ_Q:

$$\theta^I - \theta = \tan^{-1}\left(\gamma_Q\sin 2\theta\right). \tag{9}$$

The largest inhomogeneity angle occurs at, e.g., $\theta = 45^\circ$. Note that the sign of the inhomogeneity angle is governed by the attenuation-anisotropy parameter γ_Q and the phase angle θ. For example, positive γ_Q yields positive inhomogeneity angles for $0^\circ < \theta < 90^\circ$, while negative γ_Q produces negative inhomogeneity angles. Analysis of the sign of $\theta^I - \theta$ for the whole range of phase directions reveals that the attenuation vector of the SH-wave deviates toward higher-attenuation directions.

Equation 9 also shows that for weak attenuation anisotropy ($|\gamma_Q| \ll 1$), the inhomogeneity angle for SH-waves is small. Then the SH-wave attenuation can be approximately found using the expression for homogeneous wave propagation (Zhu and Tsvankin, 2006):

$$\mathcal{A}_{SH} \approx \frac{1}{2Q_{55}}(1+\gamma_Q\sin^2\theta). \tag{10}$$

3.2 P- and SV-waves

The saddle point $\tilde{\theta}_s$ for P- and SV-waves in VTI media with VTI attenuation has a more complicated form. In the limit of weak attenuation and weak anisotropy for both velocity and attenuation, the saddle-point condition for P-waves can be simplified by dropping quadratic terms in $1/Q_{33}$, $1/Q_{55}$, ϵ, δ, ϵ_Q, and δ_Q (equations B1 and B2):

$$\begin{aligned}\tan\tilde{\theta}_s = \frac{x_1}{x_3}\Big[&1-2\epsilon+2(\epsilon-\delta)\cos 2\tilde{\theta}_s\\ &+ i\frac{\epsilon_Q-(\epsilon_Q-\delta_Q)\cos 2\tilde{\theta}_s}{Q_{33}}\Big],\end{aligned} \tag{11}$$

where ϵ_Q and δ_Q are the attenuation-anisotropy parameters for P- and SV-waves (equations B1 and B2). The corresponding expression for SV-waves is

$$\tan\tilde{\theta}_s = \frac{x_1}{x_3}\left(1-2\sigma\cos 2\tilde{\theta}_s + i\frac{\sigma_Q\cos 2\tilde{\theta}_s}{Q_{55}}\right), \tag{12}$$

where $\sigma \equiv \dfrac{\epsilon-\delta}{g}$ is the velocity-anisotropy parameter for SV-waves and $g \equiv \dfrac{c_{55}}{c_{33}}$. Another parameter, $\sigma_Q \equiv \dfrac{2(1-g_Q)\sigma}{g_Q} + \dfrac{\epsilon_Q-\delta_Q}{gg_Q}$, where $g_Q = \dfrac{Q_{33}}{Q_{55}}$, governs SV-wave attenuation anisotropy (Zhu and Tsvankin, 2006). It is noteworthy that the condition for SV-waves (equation 12) can be obtained directly from that for P-waves using the following substitutions: $\epsilon \to 0$, $\delta \to \sigma$, $\epsilon_Q \to 0$, $\delta_Q \to \sigma_Q$, and $Q_{33} \to Q_{55}$.

Although the imaginary terms $\left[i\dfrac{\epsilon_Q-(\epsilon_Q-\delta_Q)\cos 2\tilde{\theta}_s}{Q_{33}}\right]$ in equation 11 and $\left(i\dfrac{\sigma_Q\cos 2\tilde{\theta}_s}{Q_{55}}\right)$ in equation 12 involve only attenuation-anisotropy parameters, the dependence of $\tilde{\theta}_s$ on the real terms makes $\theta_s^I = \mathrm{Im}[\tilde{\theta}_s]$ a function of the anisotropy parameters for both velocity and attenuation. The angle $\tilde{\theta}_s$ for P- and SV-waves is real only when the imaginary terms in equations 11 and 12, respectively, are equal to zero. For P-waves, this requires that the normalized attenuation coefficient be isotropic ($\epsilon_Q = \delta_Q = 0$). SV-wave propagation becomes homogeneous if the normalized attenuation coefficient is elliptical ($\sigma_Q = 0$). For general attenuative VTI models, $\tilde{\theta}_s$ in equations 11 and 12 can be calculated in iterative fashion. The inhomogeneity angle is then obtained from equations 2–5, as illustrated by numerical examples below.

3.3 Numerical examples

To evaluate the magnitude of the inhomogeneity angle for homogeneous attenuative VTI media, we use models 1 and 2 from Table 1. Figure 1 displays the wave vector $\mathbf{k}$ (thin arrows) and the attenuation vector $\mathbf{k}^I$ (thick arrows) for models 1 and 2. Both $\mathbf{k}$ and $\mathbf{k}^I$ are calculated with a constant increment in the group angle and displayed on the group-velocity curves (wavefronts). Notice that the wave vector remains perpendicular to the

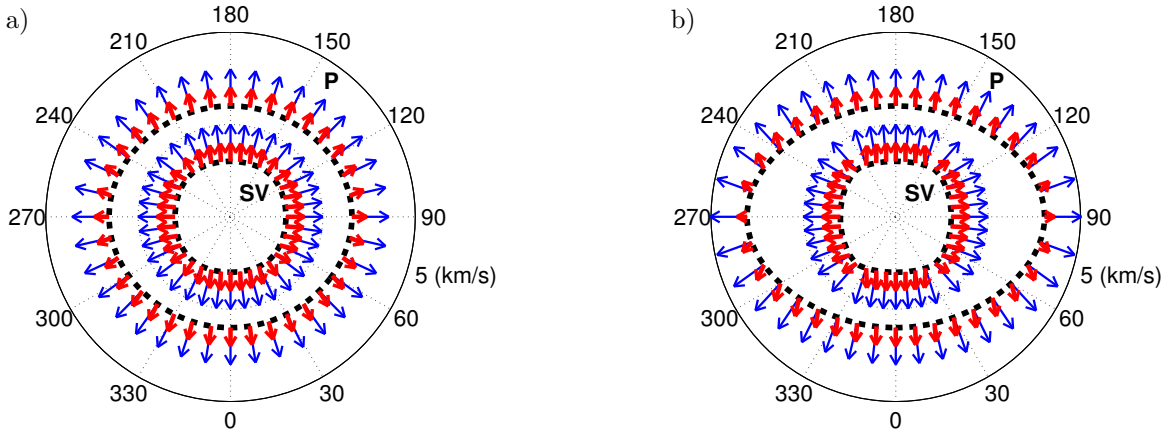

Figure 1. Polar plots of the wave vector **k** (thin black arrows) and the attenuation vector $\mathbf{k}^I$ (thick gray arrows) associated with the group-velocity curves (dashed) of P- and SV-waves for two VTI models from Table 1: a) model 1; b) model 2.

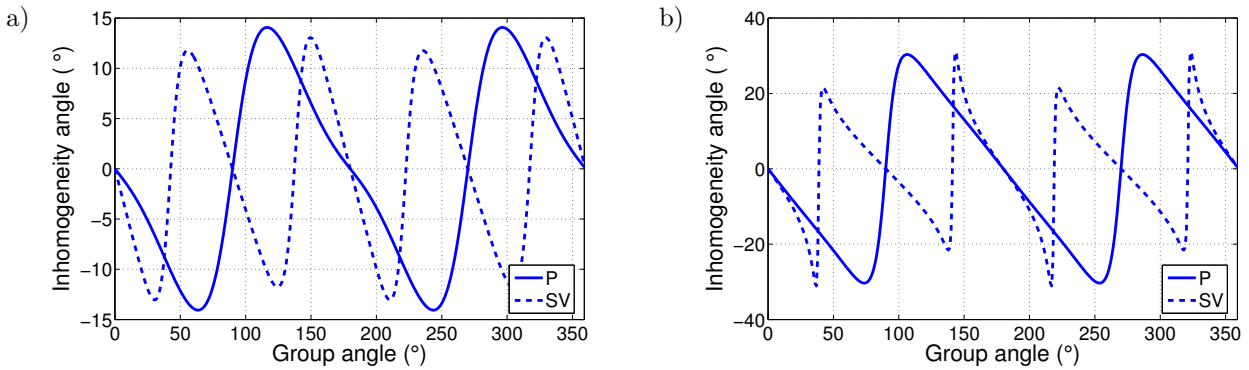

Figure 2. Exact inhomogeneity angles of P- and SV-waves for a) model 1; and b) model 2.

Model #	ϵ	δ	ϵ_Q	δ_Q
1	0.1	0.05	-0.2	-0.1
2	0.4	0.25	-0.45	-0.5
3	0.1	0.05	0	0
4	0.4	0.25	0	0
5	0	0	-0.2	-0.1
6	0	0	-0.45	-0.5

Table 1. Attenuative VTI models with $V_{P0} = 3$ km/s, $V_{S0} = 1.5$ km/s, $\rho = 2.4$ g/cm^3, $Q_{33} = 100$, and $Q_{55} = 60$.

wavefront since the influence of the attenuation on the velocity function is of the second order. The attenuation vector, however, deviates from the normal to the wavefront because of the combined influence of the velocity and attenuation anisotropy. The angle between the wave vector and the corresponding attenuation vector is equal to the inhomogeneity angle. Evidently, the inhomogeneity angle does not vanish away from the symmetry axis and isotropy plane.

The exact inhomogeneity angle computed from equation A8 is shown in Figure 2. For model 1, the inhomogeneity angles for both P- and SV-waves are less than 15° (Figure 2a). Since model 2 has stronger anisotropy for both velocity and attenuation, the inhomogeneity angles for it is larger (Figure 2b). For 2D homogeneous VTI model, the inhomogeneity angle always vanishes in the symmetry directions (0° and 90°). Figure 2b also shows that the inhomogeneity angle for SV-waves in model 2 changes rapidly near the velocity maximum at 45°, where the SV-wave wavefront becomes almost rhomb-shaped due to the large value of $\sigma = 0.6$.

Both models have negative ϵ_Q and δ_Q, which implies that the normalized attenuation for P-waves decreases monotonically from the vertical toward the hori-

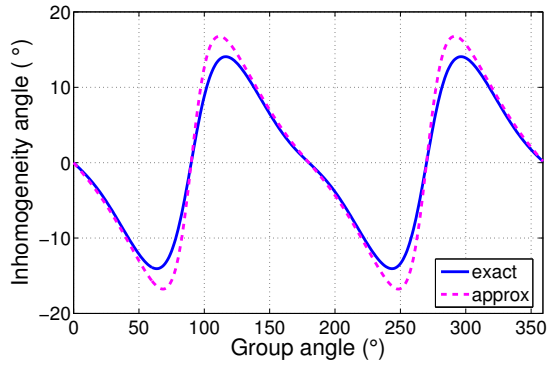

Figure 3. Comparison of the exact and approximate inhomogeneity angles for P-waves in model 1.

zontal direction. The P-wave attenuation vectors in Figure 1 are closer to the vertical direction than are the associated wave vectors. For SV-waves the attenuation vectors in model 2 deviate from the associated wave vectors toward the vertical in the range $0^\circ - 40^\circ$, where the attenuation coefficient decreases with the angle. For group angles between 50° and 90°, the opposite is true. This example, along with other numerical tests, suggests that the attenuation vector deviates from the wave vector toward the directions of increasing attenuation.

To test the accuracy of the approximate saddle-point condition for P-waves (equation 11), we compared it with the exact solution (Figure 3). The approximation generally provides sufficient accuracy, except for the directions where the term $\left.\frac{d\tilde{p}_s}{d\theta}\right|_{\theta=\tilde{\theta}_s}$ in equation A8 becomes relatively large. The overall error, however, does not exceed 4° because of the weak velocity and attenuation anisotropy for this model. Predictably, increasing the anisotropy for either the velocity or attenuation reduces the accuracy of the approximate solution.

4 RADIATION PATTERNS

Consider the wavefield from a line source in 2D attenuative anisotropic media described in the $[x_1, x_3]$-plane, where the source array function is independent of the x_2 coordinate. The spectrum of the particle displacement in the high-frequency limit, given in Appendix A, is similar to that for elastic media, but the slowness and stationary polar angle are complex. According to equation A12, anisotropic attenuation alters the radiation patterns through the geometrical spreading factor in the denominator and an exponential decaying term.

The influence of attenuation on the real and imaginary parts of the slowness $\tilde{p}_s$ is of the second and first order, respectively, in the inverse Q factors. As a result, the geometrical spreading factor depends only on quadratic and higher-order terms in the inverse Q components.

4.1 Phase and group properties

The contribution of attenuation to the radiation pattern is mostly contained in the exponentially decaying term $\exp[-\omega p^I(\sin\theta^I x_1 + \cos\theta^I x_3)]$ (equation A12). By analyzing this exponential term, we obtain the general relationship between the phase and group velocities as well as that between the phase- and group-attenuation coefficients:

$$V_G = \frac{\omega}{k_s\cos(\phi-\theta_s)\cosh\theta_s^I - k_s^I\sin(\phi-\theta_s)\sinh\theta_s^I}\,, \quad (13)$$

$$k_G^I = k_s\sin(\phi-\theta_s)\sinh\theta_s^I + k_s^I\cos(\phi-\theta_s)\cosh\theta_s^I\,, \quad (14)$$

where $k_s = \omega/p_s$, $k_s^I = \omega/p_s^I$, and ϕ is the group angle.

For homogeneous wave propagation ($\theta_s^I = 0$), the phase angle $\theta = \theta_s$ (equation 4) and the real slowness $p = p_s$ (equation 2). Hence, equations 13 and 14 reduces to (Zhu and Tsvankin, 2004)

$$V_G = \frac{V}{\cos(\phi-\theta)}\,, \quad (15)$$

$$k_G^I = k^I\cos(\phi-\theta)\,, \quad (16)$$

where $V = \omega/k$ is the phase velocity. Hence, the group attenuation coefficient for homogeneous wave propagation is equal to the phase attenuation coefficient multiplied (rather than divided, as is the case for phase velocity) by the cosine of the angle between the phase and group directions. If both functions are isotropic, the phase direction is identical to the corresponding group direction, and there is no difference between the phase and group quantities.

Since both k_s^I and θ_s^I are relatively small quantities proportional to the inverse Q factor, the influence of the inhomogeneity angle on the group velocity is of the second order in the inverse Q and can be ignored. Hence, equation 15 for the group velocity remains accurate for any value of the inhomogeneity angle. The influence of the inhomogeneity angle on the group attenuation coefficient, however, is of the first order in the inverse Q and can be significant.

4.2 Numerical examples

To examine the influence of the inhomogeneity angle on the radiation patterns and the angular variation of the phase and group attenuation coefficients as well as radiation patterns, we use VTI models from Table 1.

The contribution of the inhomogeneity angle to the P-wave attenuation coefficient is illustrated in Figure 4. The solid curves are calculated using the inhomogeneity angles obtained from Figure 2, while the dashed curves correspond to homogeneous wave propagation (i.e., zero inhomogeneity angle). Since model 1 is weakly

anisotropic for both velocity and attenuation, the inhomogeneity angle is relatively small and has a small impact on attenuation coefficients (Figure 4a). In contrast, the larger inhomogeneity angles for model 2 result in a more pronounced error in the attenuation coefficients computed for homogeneous wave propagation.

The group attenuation coefficient is also influenced by the inhomogeneity angle (Figure 5). For model 2, the attenuation coefficient computed with the actual inhomogeneity angle (equation 14) deviates by up to 20% from that for homogeneous wave propagation (equation 16).

To analyze the radiation patterns in the presence of attenuation anisotropy, we compute the particle displacement of P- and SV-waves from a vertical single force for models 1 and 2 (Figure 6). The stronger anisotropy for both velocity and attenuation in model 2 creates a more pronounced directional dependence of the radiation patterns compared to that in model 1.

Since both models have the same Q_{33} and Q_{55} values, the vertical attenuation coefficients are also the same. However, the difference between the parameter δ in the two models changes the term $\left.\frac{d^2\tilde{p}_s}{d\theta^2}\right|_{\theta=\tilde{\theta}_s}$ in equation A12 and, therefore, the magnitude of the particle displacement in the vertical symmetry direction (Tsvankin, 2005). Although the attenuation-anisotropy parameter δ_Q also contributes to the term $\left.\frac{d^2\tilde{p}_s}{d\theta^2}\right|_{\theta=\tilde{\theta}_s}$, its influence on the geometrical-spreading factor in the symmetry direction is practically negligible.

To understand the relative influence of the velocity and attenuation anisotropy on the radiation patterns, we compare the particle displacement of P- and SV-waves excited by the same vertical single force in models 3–6 from Table 1. The directional dependence of the radiation patterns for both P- and SV-waves remains pronounced even without attenuation anisotropy (Figures 7, solid curves). The radiation patterns deviate significantly from the reference isotropic values, especially for model 4 that has a particularly strong velocity anisotropy. A more detailed analysis of the P- and SV-wave radiation patterns in TI media can be found in Tsvankin (2005, chapter 2). The directional dependence of the radiation patterns becomes much less pronounced in the absence of velocity anisotropy (Figures 7, dashed curves).

Our numerical analysis confirms the well-known fact that the influence of velocity anisotropy on radiation patterns remains almost the same for different source-receiver distances. In contrast, the distortions of the radiation patterns caused by attenuation anisotropy become much more pronounced with distance because the decaying term $\exp[-\omega p^I(\sin\theta^I x_1 + \cos\theta^I x_3)]$ in equation A12 varies with the spatial coordinates (compare the dashed curves in Figure 7c,d and Figure 8).

5 DISCUSSION AND CONCLUSIONS

Wave propagation in attenuative media is generally "inhomogeneous", which means that the direction of the wave vector deviates from that of the attenuation vector. The angle between these two vectors (the "inhomogeneity angle") plays an essential role in wavefield simulation for attenuative media, especially if the velocity and attenuation functions are anisotropic. Here, we analyze the inhomogeneity angle in the far field of a line source (i.e., independent of x_2 direction) by applying the saddle-point (stationary-phase) condition to the plane-wave decomposition of the wavefield.

The discussion is largely devoted to homogeneous media with constant velocity and attenuation, where the inhomogeneity angle can be studied analytically. Although the inhomogeneity angle vanishes only in the symmetry directions, its magnitude is relatively small for weakly attenuative media with weak anisotropy for both velocity and attenuation. Therefore, for such models the attenuation coefficient can be computed under the simplifying assumption of homogeneous wave propagation. Our analysis for media with VTI symmetry for both velocity and attenuation also shows that the phase attenuation direction is shifted toward increasing attenuation.

For layered models, the take-off inhomogeneity angle at the source location can substantially change during reflection/transmission at medium interfaces. The wave vectors of reflected and transmitted waves are jointly determined by the Christoffel equation and Snell's law for attenuative media. The resulting inhomogeneity angle can be large even if the layers are weakly attenuative and are characterized by weak anisotropy for both velocity and attenuation. For a wave transmitted from a purely elastic medium into an attenuative layer, the attenuation vector is always perpendicular to the interface. For example, the inhomogeneity angle of the waves transmitted through the ocean bottom into the underwater layer with non-negligible attenuation coincides with the transmission angle (Carcione, 1999).

Along with anisotropic geometrical spreading, anisotropic attenuation in the overburden may distort the AVO (amplitude-variation-with-offset) response of reflected waves. We presented numerical examples illustrating the influence of both velocity and attenuation anisotropy on the radiation patterns. Whereas the directional amplitude variations caused by velocity anisotropy may be substantial, they do not change with source-receiver distance. In contrast, since the magnitude of the attenuation factor increases with distance, so do the amplitude distortions caused by attenuation anisotropy.

To process seismic data from attenuative media, it is necessary to relate the phase attenuation coefficient to the group (effective) attenuation along seismic rays that can be measured from recorded amplitudes. For homogeneous wave propagation, the phase velocity

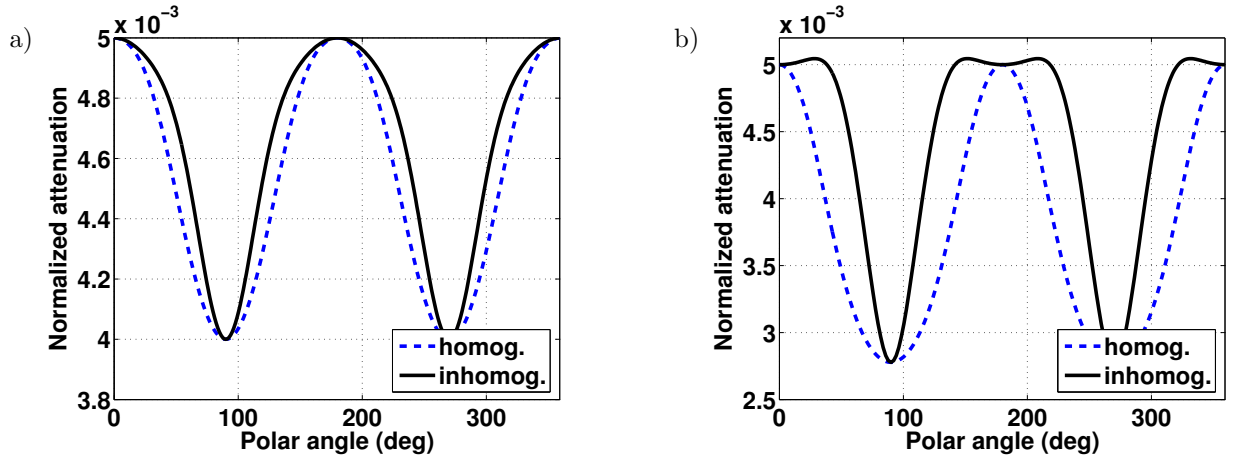

Figure 4. P-wave attenuation coefficients for a) model 1; and b) model 2. The solid curves are computed with the inhomogeneity angle from Figure 2, the dashed curves with the inhomogeneity angle set to zero for all propagation directions.

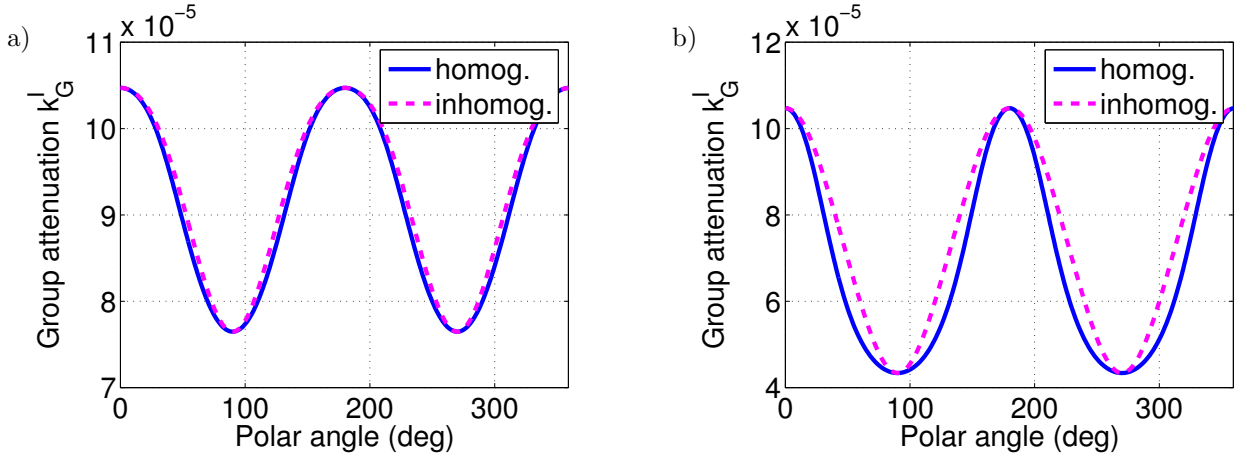

Figure 5. Group attenuation coefficients for a) model 1; and b) model 2.

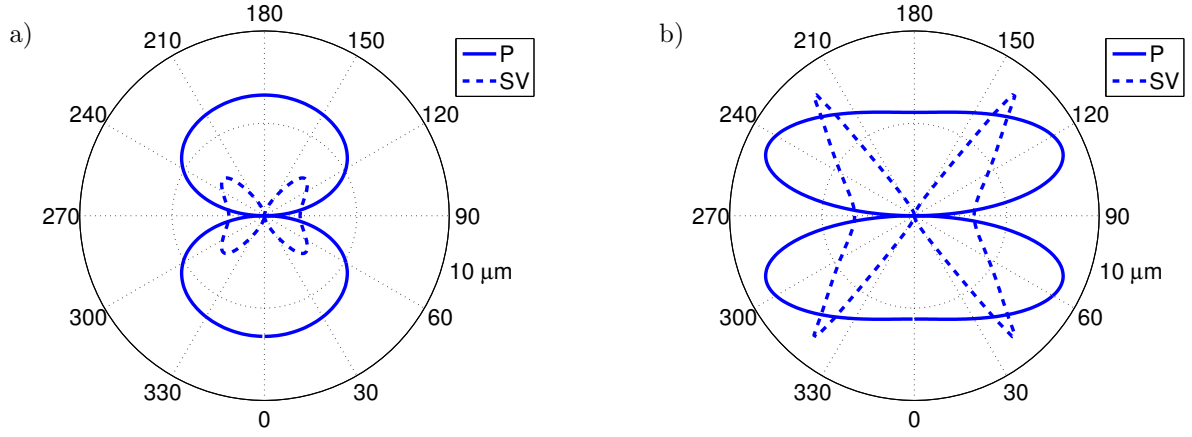

Figure 6. Radiation patterns of P-waves (solid curves) and SV-waves (dashed) from a vertical force ($f_3 = 10^5$ N) in a) model 1; and b) model 2. The magnitude of the particle displacement is computed at a distance of 1000 m away from the force; the frequency is 100 Hz.

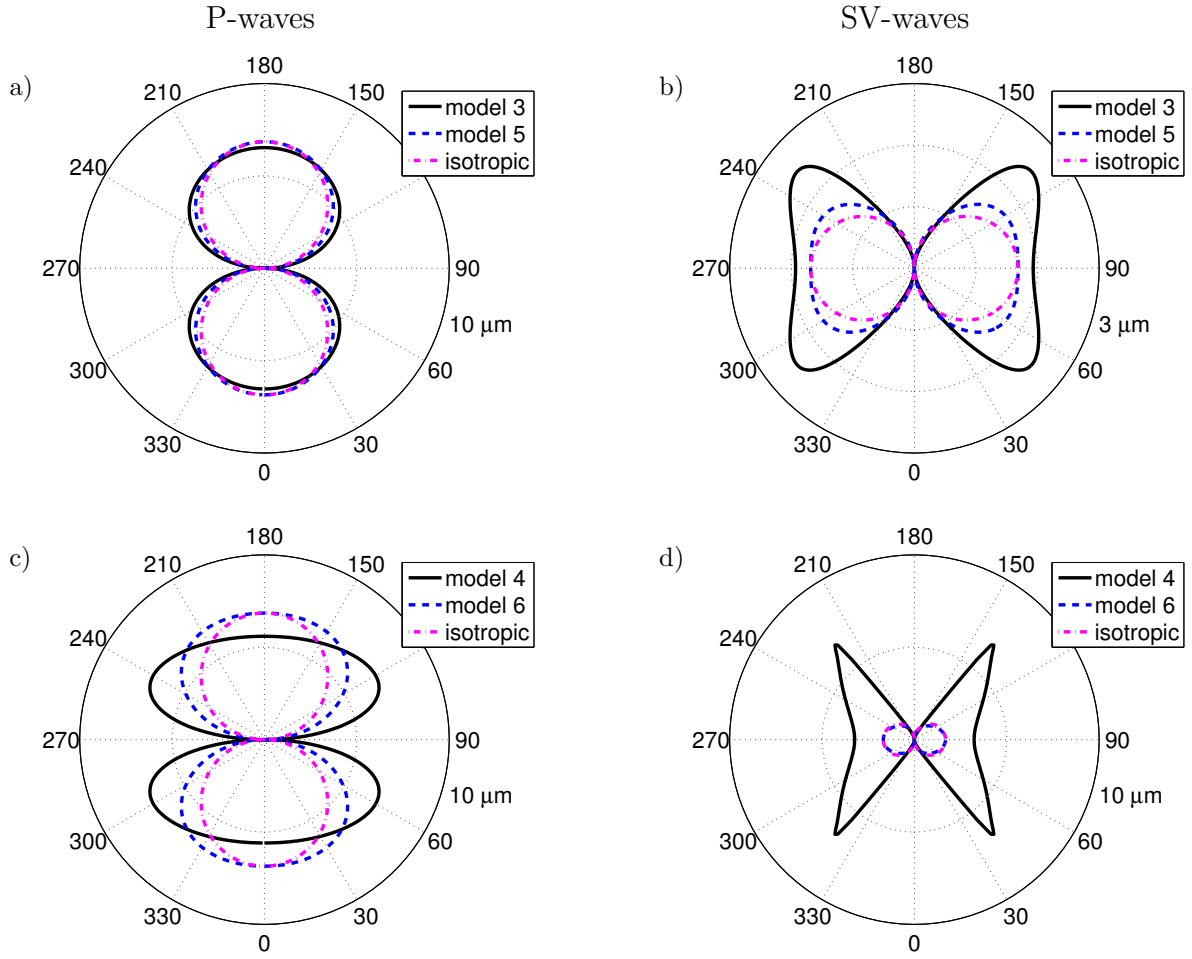

Figure 7. Radiation patterns of P- waves (left) and SV-waves (right) from a vertical force ($f_3 = 10^5$ N). The solid and dotted curves mark, respectively, the radiation patterns of P- and SV-waves for a,b) models 3 and 5 (Table 1); and c,d) models 4 and 6. The dash-dotted curves correspond to the reference isotropic models with isotropic attenuation (i.e., for $\epsilon = \delta = \epsilon_Q = \delta_Q = 0$ with the other parameters kept fixed). The source-receiver distance is 1000 m; the frequency is 100 Hz.

is equal to the projection of the corresponding group-velocity vector onto the phase direction. The relationship between the phase and group attenuation involves the same factor (the cosine of the angle between the two vectors), but it is the group attenuation that is equal to the projection of the corresponding phase-attenuation vector onto the group direction. If the inhomogeneity angle is not zero, the group velocity and attenuation depend on both the wave and phase-attenuation vectors. Still, the relationship between group and phase velocity is accurately represented by equation 15 for homogeneous wave propagation. The group attenuation coefficient, however, is described by a more complicated expression that reduces to the projection of the phase-attenuation coefficient onto the group direction only for a small inhomogeneity angle.

The analysis here was limited to 2D media, in which the attenuation vector is confined to the vertical propagation plane and governed by a single (polar) angle. Our results should be valid for any vertical plane in azimuthally isotropic homogeneous media and symmetry planes of azimuthally anisotropic media. In general, the attenuation vector in either heterogeneous or azimuthally anisotropic media is described not just by the polar angle θ^I, but also by the azimuthal angle ϕ^I. Therefore, rigorous 3D treatment of radiation patterns in anisotropic attenuative media requires application of a higher-dimensional version of the steepest-descent method.

6 ACKNOWLEDGMENTS

We are grateful to John Stockwell and members of the A(nisotropy)-Team of the Center for Wave Phenomena (CWP), Colorado School of Mines (CSM), for help-

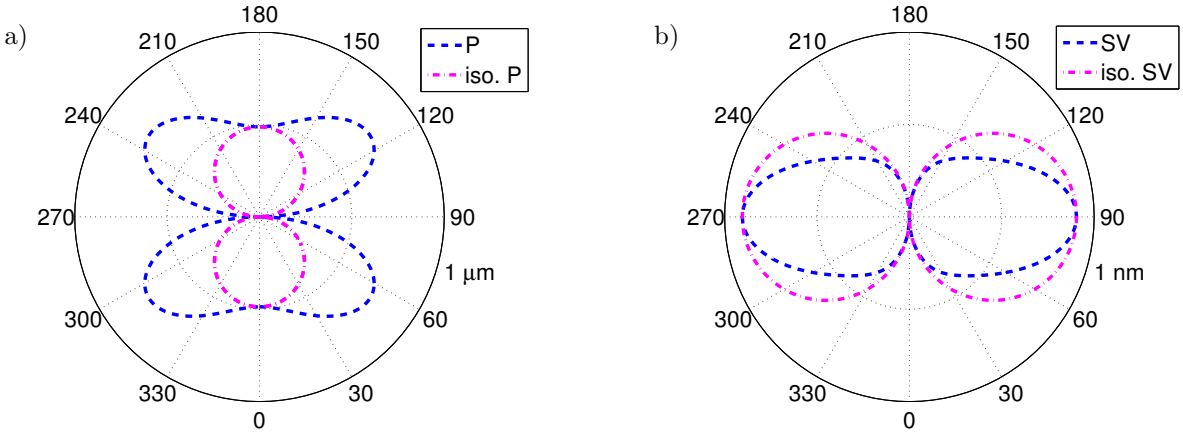

Figure 8. Radiation patterns of a) P- waves and b) SV-waves for model 6 computed at a distance of 3000 m away from the source. The dash-dotted and dotted curves mark, respectively, the radiation patterns of P- and SV-waves for the corresponding isotropic models with isotropic attenuation.

ful discussions, and to Ken Larner and Jyoti Behura (both CSM) for reviewing the manuscript. The support for this work was provided by the Consortium Project on Seismic Inverse Methods for Complex Structures at CWP.

REFERENCES

Borcherdt, R. D., and L. Wennerberg, 1985, General P, type-I S, and type-II S waves in anelastic solids; Inhomogeneous wave fields in low-loss solids: Bulletin of the Seismological Society of America, **75**, 1729–1763.

Borcherdt, R. D., G. Glassmoyer, and L. Wennerberg, 1986, Influence of welded boundaries in anelastic media on energy flow, and characteristics of P, S-I, and S-II waves: Observational evidence for inhomogeneous body waves in low-loss solids: Journal of Geophysical Research, **91**, 11503–11518.

Borcherdt, R. D., and Wennerberg, L., 1985, General P, type-I S, and type-II S waves in anelastic solids; Inhomogeneous wave fields in low-loss solids: Bulletin of the Seismological Society of America, **75**, 1729–1763.

Borcherdt, R. D., Glassmoyer, G., and Wennerberg, L., 1986, Influence of welded boundaries in anelastic media on energy flow, and characteristics of P, S-I, and S-II waves: Observational evidence for inhomogeneous body waves in low-loss solids: Journal of Geophysical Research, **91**, 11503–11518.

Carcione, J. M., 1999, Effects of vector attenuation on AVO of the offshore reflections: Geophysics, **64**, 815–819.

Carcione, J. M., 2001, Wave fields in real media: Wave propagation in anisotropic, anelastic, and porous media: Pergamon Press.

Carcione, J. M., F. Cavallini, 1995, On the acoustic-electromagnetic analogy: Wave Motion, **21**, 149–162.

Červený, V., and Pšenčík, I., 2005, Plane waves in viscoelastic anisotropic media – I. Theory: Geophysical Journal International, **161**, 197–212.

Gajewski, D., 1993, Radiation from point sources in general anisotropic media: Geophysical Journal International, **113**, 299–317.

Hearn, D. J., and E. S. Krebes, 1990, On computing ray-synthetic seismograms for anelastic media using complex rays: Geophysics, **55**, 422–432.

Krebes, E. S., and L. H. T. Le, 1994, Inhomogeneous plane waves and cylindrical waves in anisotropic anelastic media: Journal of Geophysical research, **99**, 23899–23919.

Krebes, E. S., and M. A. Slawinski, 1991, On raytracing in an elastic-anelastic medium: Bulletin of the Seismological Society of America, **81**, 667–686.

Thomsen, L., 1986, Weak elastic anisotropy: Geophysics, **51**, 1954–1966.

Tsvankin, I., 2005, Seismic signatures and analysis of reflection data in anisotropic media: Elsevier Science Publisher.

Zhu, Y., and I. Tsvankin, 2006, Plane-wave propagation in attenuative TI media: Geophysics, **71**, T17–T30.

APPENDIX A: RADIATION PATTERNS FOR 2D ATTENUATIVE ANISOTROPIC MEDIA

Here we derive an asymptotic solution for far-field radiation patterns in 2D attenuative anisotropic media using the steepest-descent method. The wave equation in the frequency-wavenumber domain can be written for wave propagation in the $[x_1, x_3]$-plane as

$$\left(\tilde{c}_{ijkl}k_jk_l - \rho\omega^2\delta_{ik}\right)\tilde{u}_k(\omega,k) = \tilde{f}_i(\omega)\,, \tag{A1}$$

where k_j are the wavenumber components, ρ is the density, ω is the angular frequency, and $i,j,k,l = 1,3$. $\tilde{u}_k(\omega,k)$ denotes the spectrum of the k-th component of the particle displacement in the frequency-wavenumber domain, $\tilde{c}_{ijkl} = c_{ijkl} - ic^I_{ijkl}$ are the complex stiffness coefficients, and $\tilde{f}_i(\omega)$ is the spectrum of the i-th component of the line source function (i.e., independent of x_2).

The spectrum of the particle displacement is given by

$$\tilde{u}_k(\omega,\mathbf{x}) = \frac{1}{(2\pi)^2}\int_{-\infty}^{\infty}\int_{-\infty}^{\infty}\frac{\tilde{f}_i(\omega)}{\tilde{c}_{ijkl}k_jk_l - \rho\omega^2\delta_{ik}}e^{i(k_1x_1+k_3x_3)}dk_1dk_3\,. \tag{A2}$$

The integral A2 can be represented in polar coordinates by using

$$p_1 = p\sin\theta;\quad p_3 = p\cos\theta\,, \tag{A3}$$

where $p = \dfrac{k}{\omega}$ is the slowness and θ is the polar angle:

$$\tilde{u}_k(\omega,\mathbf{x}) = \frac{1}{(2\pi)^2}\int_{-\infty}^{\infty}\int_{0}^{2\pi}\frac{p\tilde{f}_i(\omega)}{\tilde{c}_{ijkl}p^2n_jn_l - \rho\delta_{ik}}e^{i\omega p(x_1\sin\theta+x_3\cos\theta)}dp\,d\theta\,; \tag{A4}$$

$n_1 = \sin\theta$ and $n_3 = \cos\theta$.

Next, we apply the steepest-descent method to evaluate the integral over the slowness p. Two complex poles of the integrand correspond to the solution of the Christoffel equation:

$$\tilde{c}_{ijkl}\,p^2n_jn_l - \rho\delta_{ik} = 0\,. \tag{A5}$$

The term $\dfrac{p\tilde{f}_i(\omega)}{\tilde{c}_{ijkl}p^2n_jn_l - \rho\delta_{ik}}$ in equation A4 can be expanded in a Laurent series in terms of the slowness p, which allows us to find the residue at the pole (namely, complex slowness $\tilde{p}_s$). Equation A4 then takes the form

$$\tilde{u}_k(\omega,\mathbf{x}) = \frac{i}{2\pi}\int_0^{2\pi}\tilde{U}_k e^{i\omega\tilde{p}_s(x_1\sin\theta+x_3\cos\theta)}d\theta\,, \tag{A6}$$

where $\tilde{U}_k$ is the residue associated with a certain wave mode (P, S_1, or S_2).

The saddle-point condition corresponds to the zero derivative of the phase function:

$$\left.\frac{d\left[\tilde{p}_s(x_1\sin\theta + x_3\cos\theta)\right]}{d\theta}\right|_{\theta=\tilde{\theta}_s} = 0\,, \tag{A7}$$

and

$$\tan\tilde{\theta}_s = \frac{x_1}{x_3} + \left.\frac{d\tilde{p}_s}{d\theta}\right|_{\theta=\tilde{\theta}_s}\frac{\tilde{V}_s}{x_3\cos\tilde{\theta}_s}(x_1\sin\tilde{\theta}_s + x_3\cos\tilde{\theta}_s)\,, \tag{A8}$$

where $\tilde{V}_s = \dfrac{1}{\tilde{p}_s}$, and $\tilde{p}_s$ is obtained from the Christoffel equation at the saddle point $\tilde{\theta}_s$ (both $\tilde{p}_s$ and $\tilde{\theta}_s$ are complex). At the pole for p and the saddle point for θ, the slowness components (equation A3) are

$$\tilde{p}_1 = \tilde{p}_s\sin\tilde{\theta}_s;\quad \tilde{p}_3 = \tilde{p}_s\cos\tilde{\theta}_s\,. \tag{A9}$$

By expanding the complex phase function into a Taylor series, we found the steepest-descent direction in the vicinity of the saddle point:

$$\alpha_{\tilde{\theta}_s} = \left\{\frac{\pi}{4} - \frac{\psi}{2}, \frac{5\pi}{4} - \frac{\psi}{2}\right\}\,, \tag{A10}$$

where the perturbation on the steepest-descent direction, $\dfrac{\psi}{2}$, is the phase angle of the second derivative of the phase function at the saddle point:

$$\phi = \tan^{-1}\left[\frac{\mathrm{Im}(\tilde{Y})}{\mathrm{Re}(\tilde{Y})}\right]\,;\quad \tilde{Y} = \left.\frac{d^2\left[\tilde{p}_s(x_1\sin\theta + x_3\cos\theta)\right]}{d\theta^2}\right|_{\theta=\tilde{\theta}_s}\,. \tag{A11}$$

Evaluating the integral A6 in the high-frequency limit along the steepest descent path yields

$$\tilde{u}_k(\omega,\mathbf{x}) = \sqrt{\frac{i}{2\pi\omega}}\frac{\tilde{U}_k \exp[i\omega\tilde{p}_s(x_1\sin\tilde{\theta}_s + x_3\cos\tilde{\theta}_s)]}{\sqrt{(x_1\sin\tilde{\theta}_s + x_3\cos\tilde{\theta}_s)\left[\tilde{p}_s + 2\tilde{p}_s\left(\dfrac{x_1\cos\tilde{\theta}_s - x_3\sin\tilde{\theta}_s}{x_1\sin\tilde{\theta}_s + x_3\cos\tilde{\theta}_s}\right)^2 - \left.\dfrac{d^2\tilde{p}_s}{d\theta^2}\right|_{\theta=\tilde{\theta}_s}\right]}}\,. \tag{A12}$$

APPENDIX B: ATTENUATION ANISOTROPY PARAMETERS

The following Thomsen-style attenuation-anisotropy parameters for VTI media with VTI attenuation were introduced by Zhu and Tsvankin (2006) to simplify the description of attenuation coefficients. Although originally designed for homogeneous wave propagation, these parameters can be used to characterize attenuation anisotropy for non-zero values of the inhomogeneity angle (e.g., see equation 8).

$$\epsilon_Q \equiv \frac{1/Q_{11} - 1/Q_{33}}{1/Q_{33}} = \frac{Q_{33} - Q_{11}}{Q_{11}}\,, \tag{B1}$$

$$\delta_Q \equiv \frac{\dfrac{Q_{33} - Q_{55}}{Q_{55}}c_{55}\dfrac{(c_{13}+c_{33})^2}{(c_{33}-c_{55})} + 2\dfrac{Q_{33}-Q_{13}}{Q_{13}}c_{13}(c_{13}+c_{55})}{c_{33}(c_{33}-c_{55})}\,, \tag{B2}$$

$$\gamma_Q \equiv \frac{1/Q_{66} - 1/Q_{55}}{1/Q_{55}} = \frac{Q_{55} - Q_{66}}{Q_{66}}\,, \tag{B3}$$

where $Q_{ij} = c_{ij}/c^I_{ij}$ (no index summation) is the ratio of the real and imaginary parts of the stiffness $\tilde{c}_{ij} = c_{ij} - ic^I_{ij}$.